Journal of Solid State Chemistry 184 (2011) 2231–2237

Contents lists available at ScienceDirect

Journal of Solid State Chemistry

journal homepage: www.elsevier.com/locate/jssc

Structure and properties of a novel cobaltate $La_{0.30}CoO_2$

K. Knížek [a,*], J. Hejtmánek [a], M. Maryško [a], E. Šantavá [a], Z. Jirák [a], J. Buršík [b], K. Kirakci [b], P. Beran [c]

[a] Institute of Physics ASCR, 162 00 Prague 6, Czech Republic
[b] Institute of Inorganic Chemistry ASCR, 250 68 Rez near Prague, Czech Republic
[c] Nuclear Physics Institute ASCR, 250 68 Rez near Prague, Czech Republic

ARTICLE INFO

Article history:
Received 10 February 2011
Received in revised form
31 May 2011
Accepted 20 June 2011
Available online 28 June 2011

Keywords:
Thermoelectric cobaltates
La_xCoO_2
Na_xCoO_2
X-ray and neutron diffraction
LDA calculations

ABSTRACT

The layered cobaltate $La_{0.30}CoO_2$ was prepared from Na_xCoO_2 precursor by a solid-state ionic exchange and was characterized by means of X-ray and neutron diffraction, magnetic, thermal and electric transport measurements. The compound consists of hexagonal sheets of edge-sharing CoO_6 octahedra interleaved by lanthanum monolayers. Compared to Na^+ in the parent system, the La^{3+} ions occupy only one-third of available sites, forming a 2-dimensional superstructure. The deviation from the ideal stoichiometry $La_{1/3}CoO_2$ introduces extra hole carriers into the diamagnetic LS Co^{3+} matrix making the sample Pauli paramagnetic. The temperature dependence of the electrical conductivity in $La_{0.30}CoO_2$ follows Mott's $T^{-1/3}$ law up to about 400 K, which is in contrast with the standard metallic behavior in the Na^+ homolog possessing the same formal doping. The experiments are complemented by electronic structure calculations for $La_{0.30}CoO_2$ and related Na_xCoO_2 systems.

1. Introduction

The p-type layered cobaltates Na_xCoO_2 are promising systems for thermoelectric applications due to the high Seebeck coefficient, quasi-metallic conductivity and chemical stability at elevated temperatures. The systems are built of 2-dimensional triangular lattice sheets of cobalt ions, octahedrally coordinated with oxygen above and below the Co sheets. These CoO_2 layers are interleaved by non-conducting monolayers of variable contents of Na^+ ions (x=0–1). The stacking sequence leads to a variety of structural types of hexagonal symmetry, which differ by the number of CoO_2 layers *per* one unit cell (one, two or three) and by coordination of Na ions (mostly trigonal prismatic, sometimes octahedral), see e.g. Ref. [1]. For the electron transport properties it is important that vacant sites for $x<1$ are not distributed randomly, but are ordered according to a nanometric superstructure, which reinforces the periodic potential seen by mobile charge carriers in the conducting CoO_2 layers [2,3].

Many electric transport measurements on Na_xCoO_2 have been performed for the most stable composition x–0.7, which corresponds to a high doping of about 0.3 holes *per* Co ion. The essentially metallic character of $Na_{0.7}CoO_2$ is evidenced by in-plane resistivity, which is of low value $\sim$100 μΩ cm and increases with increase in temperature over the range 0–50 K in a quadratic manner [4]. As expected for a true metal, the thermopower coefficient increases proportionally to temperature in the low-temperature range, but tends to saturation at around room temperature, reaching a value of 70–130 μV/K.

Based on the experimental data and theoretical calculations it appears that charge carriers in the CoO_2 layer possess hole-like character and move in the background of low-spin Co^{3+} (LS, t_{2g}^6, S=0). Due to hexagonal symmetry of the constitutional layer, the orbital t_{2g} states of cobalt ions are split into the low-lying doublet e_g' and higher-lying singlet a_{1g}. The itinerant holes thus populate the lattice states of the a_{1g} parentage, which presumes, among others Ising character of their spins and explains the occurrence of a long-range antiferromagnetic ordering in some systems ($T_N\sim$22 K for Na_xCoO_2 at x=0.75–0.85 – see Ref. [5] and references therein).

Recently, analogous systems to sodium cobaltates have been prepared by the ionic exchange of monovalent sodium by divalent alkali earth (*Ae*) cations in the ratio 2:1, i.e. keeping the doping level of the parent compound [6,7]. Since Na_xCoO_2 is difficult to stabilize for $x>0.8$, and since highly charged ions can hardly be located in the monolayers so densely as Na^+, it suggests that the maximum Ca^{2+} or Sr^{2+} composition in Ae_xCoO_2 is limited to $x<0.5$. In particular, the compound $Sr_{0.35}CoO_2$ possesses not only the same formal doping of 0.3 hole *per* Co but also very analogous properties to the parent system $Na_{0.7}CoO_2$. The structures of both systems are of the so-called γ phase, characterized with two CoO_2 layers *per* one unit cell. The Sr^{2+} ions occupy trigonal prismatic coordination with oxygen ions, located at the vertical of Co triangles – the so-called *P*2 sites – in distinction to *P*1 sites (vacant in $Sr_{0.35}CoO_2$) located at the vertical of Co ions [8].

* Corresponding author.
E-mail address: knizek@fzu.cz (K. Knížek).

0022-4596/$ - see front matter © 2011 Elsevier Inc. All rights reserved.
doi:10.1016/j.jssc.2011.06.021

The present work extends the ionic exchange to trivalent lanthanide ions. In particular, we have prepared La_xCoO_2 system for $x=0.30$, i.e. close to the diamagnetic purely Co^{3+} cobaltate. The compound shows a distribution of La^{3+} ions over one-third of the *P*2 sites, forming a 2-dimensional quasi-hexagonal $a\sqrt{3}\times a\sqrt{3}$ superstructure. The results of LDA calculations, magnetic susceptibility, specific heat and thermopower point to the presence of hole carriers in a narrow band. In distinction to metallicity in Na_xCoO_2 systems of the same doping of 0.10 holes *per* Co, the conductivity in $La_{0.30}CoO_2$ is of Mott's variable range hopping. The compound can be thus characterized as Pauli paramagnet with significant disorder.

2. Experimental

The parent compound $NaCoO_2$ has been prepared by a soft chemistry route (Pechini process) according to the following procedure: calculated amounts of $NaNO_3$ and $Co(CH_3COO)_2\cdot 4H_2O$ (corresponding to 5% surplus in Na relative to the ideal $Na_1Co_1O_2$ stoichiometry) were decomposed by diluted HNO_3. The amount of HNO_3 in this solution did not exceed the minimum amount needed for complete decomposition of Co(II) acetate, and also the amount of H_2O was kept at the minimum needed for obtaining clear and transparent solution of metal nitrates. Then, water solution of ethyleneglycol (EG) with citric acid (CA) was added slowly under continuous mixing and heating. The molar composition of resulting precursor solution was $(NO_3)^-$:EG:CA= 1:1:1. The gelation reaction was accomplished in drying chamber at 110 °C. After several hours of drying, voluminous foam of precursor gel was broken into fine powder and pyrolysed at 350 °C in the furnace. The crystallization of nominally $NaCoO_2$ phase was done by annealing at 800 °C for 3 days in air. Then, the new phase with composition La_xCoO_2 was prepared by intercalation reaction between $NaCoO_2$ and $La(NO_3)_3$, facilitating the ionic exchange $3Na^+\leftrightarrow La^{3+}$ according to the following procedure: $NaCoO_2$ was thoroughly mixed with anhydrous $La(NO_3)_3$ (10% surplus in La content relative to theoretical composition $La_{0.33}CoO_2$) in dry-box under N_2 atmosphere and the reaction mixture was placed into the furnace preheated to 250 °C. Reaction mixture in crucible capped with alumina plate was heated at 300 °C for 2 days. During this time, the mixture was re-mixed several times to reach good intermixing of reacting solid phases. Then, the unreacted $La(NO_3)_3$ was washed out repeatedly with large amount of cold water and using ultrasonic treatment. The final product was dried at 110 °C in air for 16 h.

The X-ray fluorescence (XRF) analyses of chemical compositions of the starting Na_xCoO_2 and final La_xCoO_2 materials were done using X-ray spectrometer ARL 9400 XP.

Powder X-ray diffraction patterns were recorded with a Bruker D8 diffractometer with Cu*K*α radiation (λ=1.5418 Å) and SOL-X energy dispersive detector. The neutron powder diffraction pattern was recorded on instrument MEREDIT [9] in Nuclear Physics Institute in Rez near Prague. Planes (220) of mosaic copper crystals were used as monochromator providing neutron wavelength of 1.460 Å. Data were collected between 4° and 148° of 2θ with the step of 0.08°. Time delay on each step was controlled by monitor and was about 470 s. Structural refinements were done by Rietveld profile analysis using program FULLPROF [10] (version 4.80—Jan2010-ILL JRC).

The magnetic experiments were carried out using Quantum Design DC superconducting quantum interference device (SQUID) MPMS XL magnetometer. They included the measurements of the ZFC and FC susceptibility under an applied field 10 kOe and isothermal magnetization curvess 0–50 kOe—0 recorded at selected temperatures. The specific heat was measured by PPMS device (Quantum Design) using the two-τ model. The data were collected on sample cooling.

The electrical resistivity, thermoelectric power and thermal conductivity were measured on samples cold-pressed into dense pellets. In the low-temperature range, a homemade apparatus and a close-cycle cryostat working down to 2–3 K were used [11]. The electrical current density varied depending on the sample resistivity between 10^{-1} and 10^{-7} A/cm^2 (for the most insulating state). The four-point steady state method for both the resistivity and the thermopower was applied and the measurements were done on sample cooling and warming. For the high temperature measurements the samples were placed on the ceramic sample holder centered in the small tubular furnace with precisely controlled temperature. The standard S-type thermocouples (Pt–PtRh10%) were used for monitoring the temperature gradient around 3 K, imposed across the sample by means of an additional small furnace. In the high-temperature measurements, the four-point steady state method for resistivity and thermopower was applied, as well.

The local density approximation (LDA) calculations were done with the WIEN2k program [12]. This program is based on the density functional theory (DFT) and uses the full-potential linearized augmented plane wave (FP LAPW) method with the dual basis set. The core states were defined as electronic configuration (Kr, $4d^{10}$) for La, (Ne, $3s^2$) for Co, and as (He) for Na and O atoms. The radii of the atomic spheres were taken 2.3 a.u. for La and Na, 1.9 a.u. for Co and 1.6 a.u. for O. The number of *k* points in the irreducible part of the Brillouin zone was 320 for $P6_3/mmc$ and 192 for *Cmcm* cell.

The physical experiments were generally performed on samples that showed no trace of impurity in the X-ray diffraction patterns (in particular the La_xCoO_2 sample A). In order to separate the intrinsic magnetic susceptibility, complementary experiments were done also on the sample with certain amount of parasitic phase—La_xCoO_2 sample B. This parasitic phase was identified using XRD analysis as spinel Co_3O_4 by the presence of two very weak peaks in X-ray diffraction pattern. We have confirmed that this impurity appears after additional annealing of the material at 300 °C. Finally, additional experiments unveiled that annealing the La_xCoO_2 above 400 °C in air leads to a decomposition.

3. Results

3.1. Composition, crystal structure and electronic density functional calculations

The X-ray diffraction on the parent Na_xCoO_2 compound revealed a single γ phase of hexagonal $P6_3/mmc$ symmetry with lattice parameters refined to $a=2.837$ Å and $c=10.855$ Å. The type of the structure and the values of lattice parameters are characteristic for x–0.75 according to the literature data [13,14]. This composition is markedly smaller than the total sodium content in sample, $x=0.90$, determined by XRF analysis. This suggests that a part of sodium has been segregated from the cobaltate phase.

In the case of La_xCoO_2, the relevant data on lanthanum content were obtained independently from refinements of X-ray and neutron diffraction data, which gave consistently $x=0.30(1)$, suggesting a doping of 0.10(3) hole *per* Co. Moreover, the XRF analysis of total lanthanum content in the sample yielded the same composition. In the same experiment, certain amount of residual sodium, presumably segregated from the cobaltate phase, was also detected. The X-ray diffraction pattern of sample A is presented in the lower panel of Fig. 1. It shows fundamental lines corresponding to the $P6_3/mmc$ structure of γ phase with

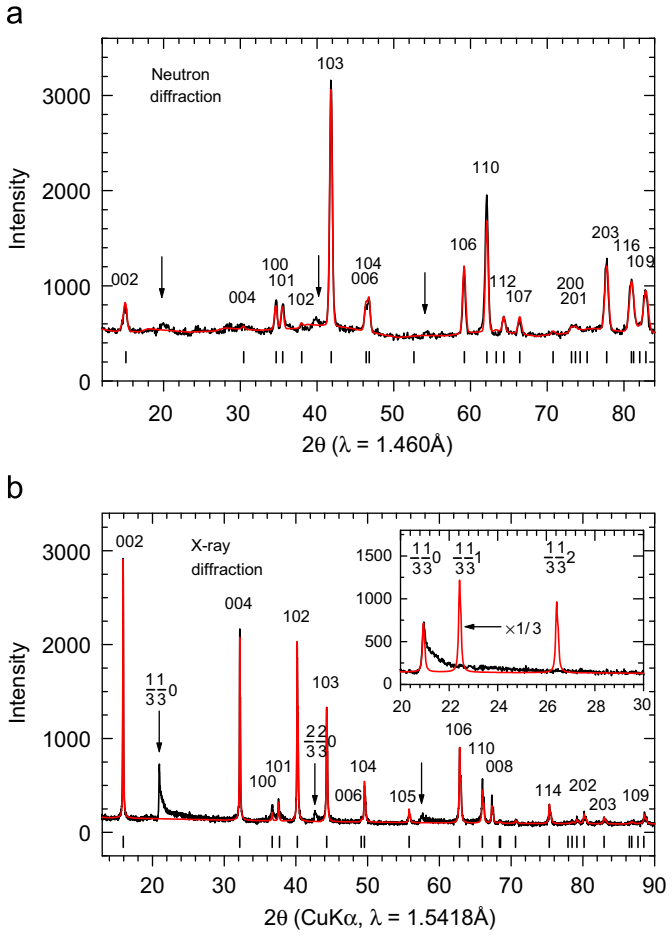

Fig. 1. The neutron (a) and X-ray diffraction (b) patterns of the $La_{0.30}CoO_2$ sample A. The arrows mark highly asymmetric peaks due to a short-range lanthanum ordering. The most intense peak at the position $\frac{1}{3}\frac{1}{3}0$ is shown in detail in the inset and is compared with the calculated diffraction lines for a model of 3-dim. superstructure in $La_{1/3}CoO_2$.

lattice parameters $a=2.8290(1)$ Å and $c=11.1205(8)$ Å. In addition, some highly asymmetric extra peaks are detected. They show a sharp edge from the low 2θ side of the calculated position for superstructure lines $\frac{1}{3}\frac{1}{3}0$ and $\frac{2}{3}\frac{2}{3}0$, and a long tail to higher 2θ. This observation is a strong signature for ordering of La ions in the present La_xCoO_2 system close to the ideal composition $x=1/3$, in which the occupation of neighboring $P2$ positions at $a=2.83$ Å is avoided due to electrostatic repulsion, and, consequently, a regular hexagonal array with La–La distance of $\sqrt{3}a=4.90$ Å is formed. The long tail for superstructure peaks $\frac{h}{3}\frac{h}{3}0$ and apparent absence of superstructure peaks with $l\neq 0$ then suggest that the actual ordering is 2-dimensional, characterized in the reciprocal space by diffraction bars instead of common points. The interplanar correlations are only of a short range (in each La plane there are three-ordered variants possible). In the neutron diffraction pattern (see upper panel of Fig. 1) similar superstructure peaks are observed. But they are of relatively weaker intensity because neutron scattering amplitude of La is comparable with that of oxygen and cobalt while X-ray diffraction is very sensitive to heavy La atoms.

If the superstructure was 3-dimensionally ordered, the symmetry would be orthorhombic *Cmcm* with a pseudo-hexagonal primitive cell of dimensions $\sqrt{3}a\times\sqrt{3}a\times c$ ($\mathbf{a}_O=-3\mathbf{b}_H$, $\mathbf{b}_O=2\mathbf{a}_H+\mathbf{b}_H$, $\mathbf{c}_O=\mathbf{c}_H$). With a loss of ordering along the *c*-axis, the average $P6_3/mmc$ structure can only be refined. The results of combined FULLPROF analysis of neutron and X-ray diffraction patterns are

Table 1
Structural parameters and selected bond lengths and angles of $La_{0.30}CoO_2$ refined by Rietveld method within the hexagonal space group $P6_3/mmc$ using combination of X-ray and neutron diffraction. Atom coordinates: La $2d$(1/3.2/3.3/4), Co $2a$(0.0.0), O $4f$(1/3.2/3,z). Agreement factors: $R_p=3.87$, $R_{wp}=5.07$, $\chi^2=3.03$ (neutron diffraction); $R_p=8.79$, $R_{wp}=11.2$, $\chi^2=1.61$ (X-ray diffraction).

a (Å)	2.8290(1)	La, occupation	0.30(1)
c (Å)	11.1205(8)	Co–O (Å) × 6	1.924(2)
La, B_{iso} (Å^2)	0.10(9)	La–O (Å) × 6	2.404(3)
Co, B_{iso} (Å^2)	0.07(6)	O - Co–O (deg.)	94.7(2)
O, B_{iso} (Å^2)	0.14(6)	O - La–O (deg.)	72.1(1)
O (z)	0.0914(4)	Co–O - La (deg.)	164.7(2)

presented in Table 1. The in-plane order and the oxygen coordination of lanthanum in the prismatic $P2$ sites are depicted in Fig. 2. Within the average structure, the La–O distance is 2.404(3) Å, which is slightly shorter than expected for La^{3+} in the six-fold trigonal prismatic coordination. This suggests that the oxygen sites in CoO_2 layers adapt to the real alternation of occupied and unoccupied La positions. In order to quantify the atomic displacements due to the La ordering, an optimization was performed for the actual composition $La_{0.30}CoO_2$ by electronic structure calculations using LDA method. The concentration of 0.10 holes *per* Co ion was simulated by a virtual atom method ($Z=56.7$ for La in $LaCo_3O_6$ formula). The refined atomic coordinates relevant to the base centered *Cmcm* unit cell are presented in Table 2. Minor shifts are only obtained compared to the average $P6_3/mmc$ structure, resulting in two distinct Co–O bond distances, which differ by 0.02 Å (see Fig. 2). In addition to the main trigonal CoO_6 distortion characterized by the O–Co–O angle of 94.7°, the Co1 centered octahedron possesses a slight tetragonal compression along the main diagonal while the Co2 sites are shifted off center.

The spin unpolarized solution for the *Cmcm* superstructure is presented by the calculated density of states (DOS) in Fig. 3 and is compared with the results for the $P6_3/mmc$ structure of Na_xCoO_2 at the same hole doping, i.e. $x=0.90$, locating sodium ions in the $P2$ sites.

The main features of the band structure are essentially the same for both systems. The band of Co t_{2g} parentage, split by trigonal distortion of CoO_6 octahedra into a_{1g} and e_g manifolds, spreads from about $+0.1$ to -1.3 eV. The unoccupied band of e'_g parentage is located at 1.2–2.2 eV above E_F. The band of oxygen parentage is separated by a small gap from the t_{2g} one and spreads from -2 to -7 eV. Narrow band of La parentage is located deeply below E_F at -14 eV, and the unoccupied one at $+5$ eV.

More marked differences between La and Na cobaltates can be seen in the form of Fermi surface, sketched by the $k_z=0$ cut in Fig. 4. The top of the t_{2g} band is constituted exclusively by the anti-bonding combinations of the cobalt a_{1g} orbitals (the $(d_{xy}+d_{yz}+d_{zx})/\sqrt{3}$ eigenfunctions). For $Na_{0.90}CoO_2$, these orbitals form Fermi surface of toroidal shape, which is viewed close to the $k_z=0$ plane as two concentric portions around the Γ point (see the right-hand picture of Fig. 4)—the outer part of hole character and the inner part of electron character. The $\sqrt{3}a\times\sqrt{3}a$ superstructure in $La_{0.30}CoO_2$ brings about further modification, most readily seen by a larger diameter of the inner electron part. This leads to a smaller electron free area between two rings, which is compensated by larger thickness of the toroid in the k_z direction (not shown in Fig. 4). By closer inspection, one may also find that the hole Fermi surface is somewhat more wrapped and slightly compressed along the orthorhombic $\mathbf{b}^*_O$ axis. According to our supplementary calculations, the toroidal Fermi surface in cobaltates with 10% hole doping evolves with increase in doping towards a standard cylindrical sheet along the k_z axis. The inner

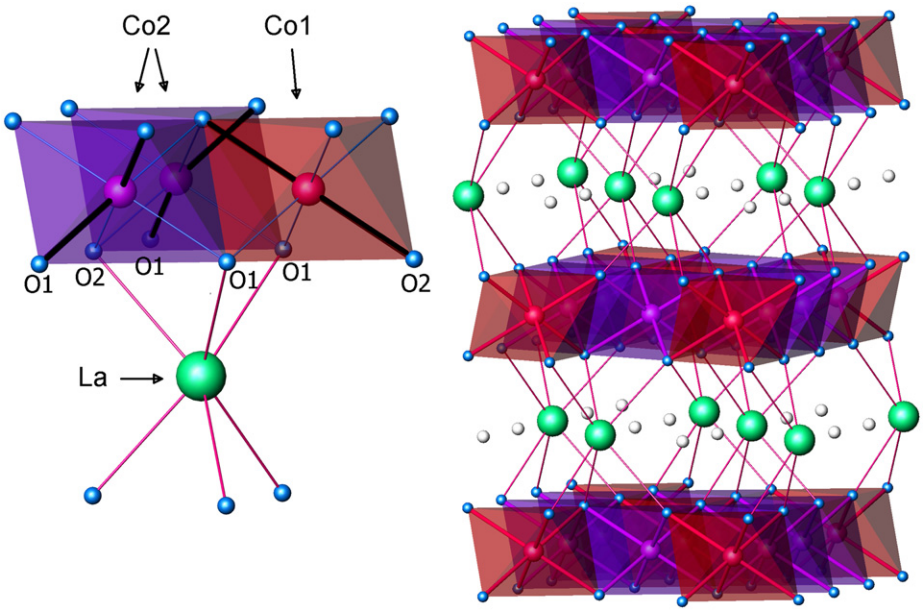

Fig. 2. The ideal *Cmcm* structure of $La_{1/3}CoO_2$. Left picture illustrates the bonding between La ion in the prismatic coordination and Co1 and Co2 ions in octahedral coordination. Some Co–O bonds in the octahedra are shortened upon the lanthanum ordering as marked by heavy lines (see also Table 2).

Table 2
Structural parameters and selected bond lengths of $La_{0.30}CoO_2$ supercell optimized by LDA calculation within the orthorhombic space group *Cmcm*. Relations between the orthorhombic and the hexagonal lattice vectors are $\mathbf{a}_O=-3\mathbf{b}_H$, $\mathbf{b}_O=2\mathbf{a}_H+\mathbf{b}_H$, $\mathbf{c}_O=\mathbf{c}_H$). Atom coordinates: La 4*c*(0,*y*,1/4), Co1 4*a*(0.0.0), Co2 8*e*(*x*,0.0), O1 16*h*(*x*,*y*,*z*), O2 8*f*(0,*y*,*z*).

a (Å)	8.4870	Co1–O1 (Å) × 4	1.918
b (Å)	4.9000	Co1–O2 (Å) × 2	1.897
c (Å)	11.1205	Co2–O1 (Å) × 2	1.897
La (*y*)	0.3325	Co2–O1 (Å) × 2	1.918
Co2 (*x*)	0.3329	Co2–O2 (Å) × 2	1.917
O1 (*x*)	0.1681	La–O1 (Å) × 4	2.429
O1 (*y*)	0.1652	La–O2 (Å) × 2	2.437
O1 (*z*)	0.0893		
O2 (*y*)	0.6694		
O2 (*z*)	0.0888		

part of the toroid is strangulated at the Γ point for composition of about $Na_{0.7}CoO_2$ and finally forms an electron pocket centered at the A point of Brillouin zone (in the $k_z=1/2$ plane).

In order to investigate a tendency to magnetic ordering in $La_{0.30}CoO_2$, the spin-polarized calculation was done, as well (see also Ref. [15]). Such solutions were lower in energy relative to the unpolarized one by 2 meV/Co ion, only. Such small difference and naturally 2-dimensional character of magnetic interactions make eventual FM or A-type AFM ordering unlike. As a consequence the compounds of 10% hole doping can be viewed as Pauli metals.

3.2. Magnetic susceptibility and the low-temperature specific heat

The magnetic properties of weakly doped cobaltates are associated with hole carriers of spin 1/2, which are introduced into diamagnetic background of LS Co^{3+}. As a consequence, the data actually measured are definitely affected by the presence of magnetically stronger impurities. A common parasitic phase in samples prepared at relatively low temperatures is the Co_3O_4 phase, which possesses a normal spinel structure with non-magnetic LS Co^{3+} ions in octahedral sites and magnetic Co^{2+} ions in tetrahedral sites. The bulk Co_3O_4 orders antiferromagnetically at low temperature ($T_N=30$ K), nonetheless due to a

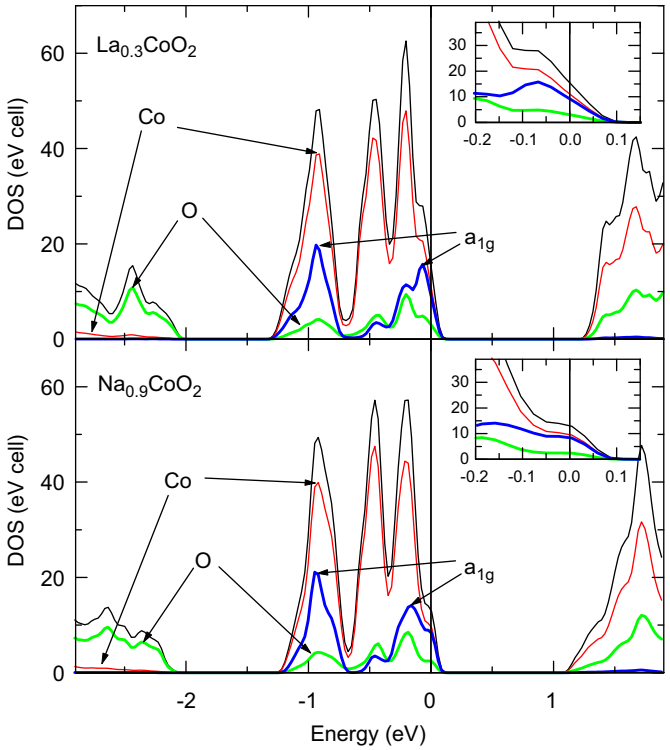

Fig. 3. LDA paramagnetic DOS of the ordered structure of hole doped $La_{0.30}CoO_2$. Results for $Na_{0.90}CoO_2$ of the same doping are added for comparison. The arrows show the partial Co and O densities and the location of states of prevailing a_{1g} character (see text).

complexity of magnetic interactions, the simple AFM ordering is substantially modified in nanosize particles, namely because of their partially inverted cationic distribution. Moreover with further size reduction below ~2 nm even a sizeable ferrimagnetic moment can appear at low temperatures [16,17].

As present $La_{0.30}CoO_2$ system is concerned, the parasitic magnetism largely obscures the intrinsic susceptibility, even in sample A with no trace of Co_3O_4 impurity in the X-ray diffraction

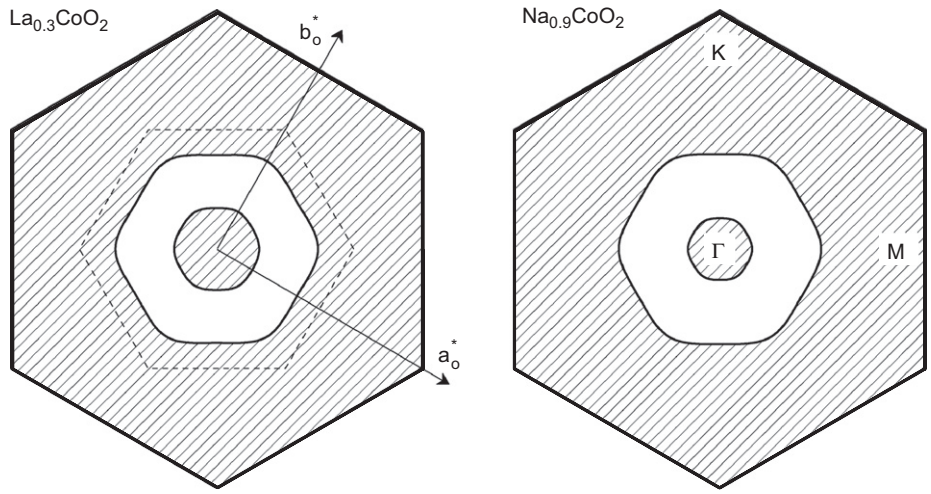

Fig. 4. The shape of Fermi surface in $La_{0.30}CoO_2$, shown in the Brillouin zone relevant to the $P6_3/mmc$ substructure. The true Brillouin zone of the orthorhombic *Cmcm* structure is marked by the dashed lines. The right-hand picture shows Fermi surface in the hexagonal $Na_{0.90}CoO_2$.

pattern. In that case the impurity contribution has a typical ferrimagnetic character of the susceptibility, pointing to the presence of Co_3O_4 in the form of finely dispersed matter or intergrowth layers. Though the total impurity amount in sample A need not be large, we found impossible to separate the intrinsic susceptibility of $La_{0.30}CoO_2$.

The DC susceptibility data measured at $H=10$ kOe on sample B are presented in Fig. 5. According to the diffraction data, this sample contains 8 mol% of crystalline Co_3O_4, which presence is evidenced in the susceptibility data by a clear anomaly at $T_N=30$ K. Despite the rather high contamination, the intrinsic and impurity contributions can be separated with reasonable reliability considering their different temperature behaviors. For the cobaltate, at least in the regime of the low doping considered, the main contribution is the temperature independent term due to Van Vleck and/or Pauli susceptibility, and a weak Curie term due to minor localized spins. On the other hand, the paramagnetic contribution due to Co_3O_4 is definitely characterized by Curie–Weiss term with AFM interactions. For the sake of experimental credibility of the above outlined analysis we performed a reference measurement of susceptibility on Co_3O_4 commercial nanopowder (Aldrich, average particle size ~25 nm). A standard analysis using the formula $\chi=C/(T-\theta)+\chi_0$ applied to the paramagnetic region (above ~80 K) provided an effective moment of $\mu_{eff}=4.35\ \mu_B$ and antiferromagnetic Weiss temperature $\theta=-80$ K and $\chi_0=3\times10^{-6}$ emu g^{-1} Oe^{-1} (0.7×10^{-3} emu mol^{-1} Oe^{-1}) values, which are very close to the values reported for bulk material [18]. Considering these experimental characteristics the data of sample B allows us to discriminate intrinsic susceptibility of $La_{0.30}CoO_2$ by fitting the amount of Co_3O_4 impurity. This analysis is depicted in Fig. 5 when the amount of Co_3O_4 impurity was refined to 12 wt% (7 mol% Co_3O_4) in a perfect agreement with the result of X-ray diffraction analysis.

The refined $La_{0.30}CoO_2$ susceptibility consists of temperature independent part and, in addition, of a minor Curie term $\chi=C/T$ seen as a diverging low-temperature tail. Its magnitude points to a presence of 0.01 localized spins 1/2 per Co, i.e. only one-tenth of total hole doping. The dominating temperature independent susceptibility $\chi_0=2.3\times10^{-4}$ emu mol^{-1} Oe^{-1} originates of three contributions—Van Vleck paramagnetism, orbital diamagnetism and, finally, considering the finite DOS at Fermi level in LDA solution, Pauli paramagnetism. We note that the fit for sample B in Fig. 5 is robust and significant. Namely, supposing that the amount of Co_3O_4 was increased above 7 mol%, the $La_{0.30}CoO_2$ susceptibility component would increase with temperature, which is very improbable. On the other hand, fixing a lower

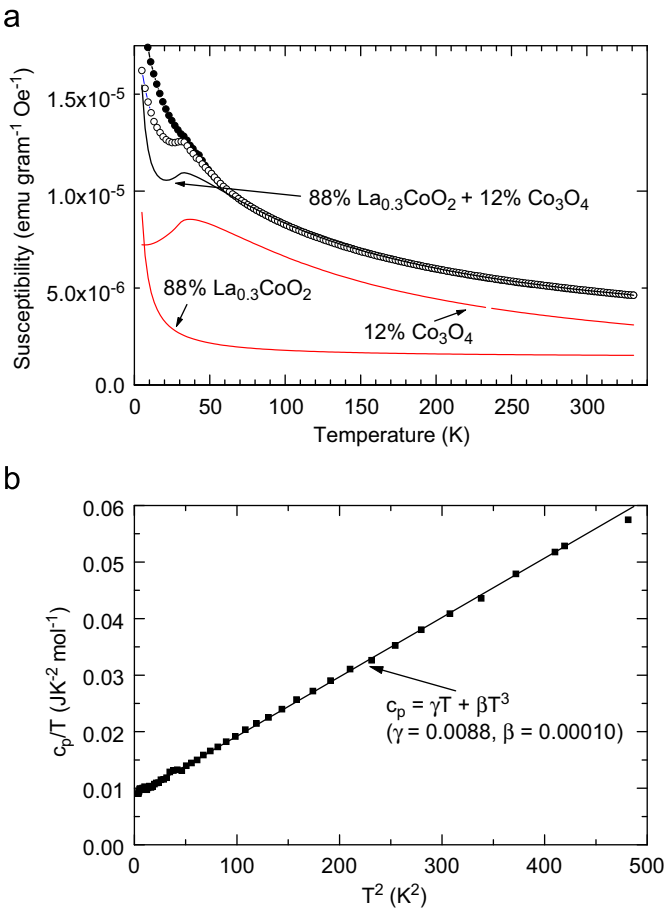

Fig. 5. (a) ZFC and FC susceptibility measured on the $La_{0.30}CoO_2$ sample B (open and solid symbols). The fit shown by full lines resolves two contributions—the intrinsic one and that of 12 wt% Co_3O_4 impurity (see text). (b) The low-temperature specific heat of $La_{0.30}CoO_2$ in the c_p/T vs. T^2 plot.

Co_3O_4 amount in the sample would lead to a larger number of localized spins, which would make a large discrepancy with the observed low-temperature tail.

An additional experimental evidence of finite DOS at Fermi level, supported by the above mentioned Pauli paramagnetism, comes from the low temperature specific heat data. The observation shown

in Fig. 5b points to an existence of linear term $c_p=\gamma T$ with Sommerfeld coefficient $\gamma=0.0088\ \mathrm{J\,K^{-2}\,mol^{-1}}$. This is a value commonly observed for electronic specific heat in the low-doped metallic cobaltates Na_xCoO_2 [19], which confirms independently the barely metallic nature of this novel $La_{0.30}CoO_2$ compound. Finally, the second low-temperature component βT^3 refers to phononic heat and the observed value $\beta=0.00010\ \mathrm{J\,K^{-4}\,mol^{-1}}$ corresponds to very reasonable Debye temperature of about 400 K.

3.3. Transport properties

The resistivity, thermopower and thermal conductivity data on $La_{0.30}CoO_2$ are presented in Fig. 6 together with data for parent compound Na_xCoO_2 (x–0.75) and reference ceramic sample $Na_{0.90}CoO_2$. We note that the transport properties are identical for $La_{0.30}CoO_2$ samples A and B, and, moreover, the cold-pressed samples show apparently the same absolute resistivity values as samples sintered at 300 °C. We relate the very good compactness and electrical connectivity in cold-pressed samples to a plasticizing effect of extra-granular sodium.

The results in Fig. 6a show that the temperature dependence of resistivity in the cold-pressed $Na_{0.75}CoO_2$ sample is metallic-like, similar to the in-plane resistivity in single crystals [4]. The absolute values are, however, to 1–2 order magnitude larger, which can be associated with much shorter mean free path of charge carriers. On the other hand, the resistivity of $La_{0.30}CoO_2$ exhibits a clear localization towards low temperatures and

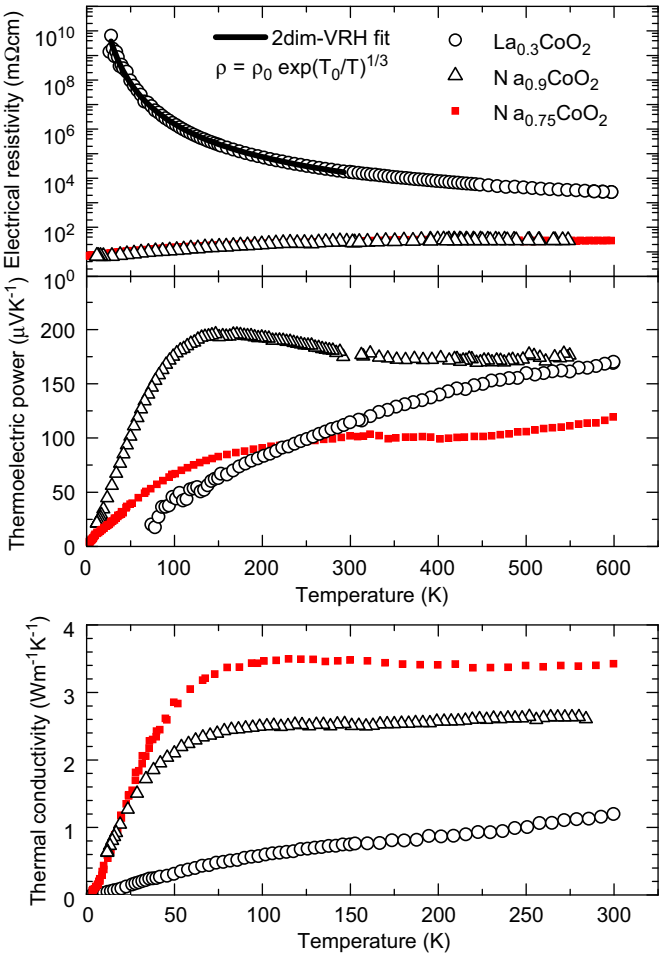

Fig. 6. The temperature dependence of thermopower, resistivity and thermal conductivity in $La_{0.30}CoO_2$. The same data of $Na_{0.9}CoO_2$ and $Na_{0.75}CoO_2$ are added for comparison.

follows a temperature dependence $\rho(T)=\rho(0)\exp\{(T/T_0)^{-1/n}\}$. The fractional exponent is characteristic for a regime of variable-range hopping (VRH), inherent to disordered systems, in which hopping occurs between Anderson localized states near Fermi level and involves also quantum tunneling to more distant lower-energy sites. The present fit gives $n=3$, which is exactly the value corresponding to 2-dimensional transport in Mott's VRH theory. The remaining parameters in the fit are $\rho(0)=0.53\ \mathrm{m\,\Omega\,cm}$ and $T_0=360{,}000$ K.

Despite the obvious localization in $La_{0.30}CoO_2$, the system shows a quasi-linear (metallic-like) rise of thermopower. The slope is however, not so steep as in the similarly doped $Na_{0.90}CoO_2$ (Fig. 6b). At high temperatures, however, the thermopower data in both systems with 10% of hole doping tend to the same value of $\sim$200 μV/K. This value is very close to the theoretical Heikes' limit 189 μV/K for 10% hole doping disregarding the spin entropy contribution. In coherence with the literature data, the parent compound $Na_{0.75}CoO_2$ shows significantly smaller thermopower due to higher charge-carrier concentration.

The temperature dependence of the total thermal conductivity, κ_{total}, is shown in Fig. 6c. At room temperature κ_{total} is in the range of 2.6–3.4 $\mathrm{W\,m^{-1}\,K^{-1}}$ for Na based cobaltates, while that of $La_{0.30}CoO_2$ amounts to $\sim$ 1 $\mathrm{W\,m^{-1}\,K^{-1}}$ only. Supposing the conventional analysis, the total thermal conductivity can be expressed as $\kappa_{total}=\kappa_{el}+\kappa_{ph}$, where κ_{ph} is the phononic contribution and κ_{el} is the electronic contribution, which can be estimated using the Wiedemann–Franz law: $\kappa_{el}=L_0\sigma T$ ($L_0=2.443\times10^{-8}$ is the Lorenz number for free electron gas, σ is the electrical conductivity and T is the absolute temperature). Considering thus the electrical conductivity from Fig. 6a, the κ_{el} is negligible and the phononic part κ_{ph} dominates the thermal conduction. In connection with cold-pressing technology of the sample preparation we just note that, apparently, the fact that samples are only "cold pressed", i.e. without subsequent sintering, does not influence the thermal conductivity so fundamentally as one can suspect.

4. Discussion and conclusions

A novel cobaltate $La_{0.30}CoO_2$ has been prepared by a solid state ionic exchange starting from the sodium cobaltate. The structure of $La_{0.30}CoO_2$ is of a two-layer type of hexagonal $P6_3/mmc$ symmetry, the so-called γ phase. Compared to a complex distribution of Na^+ over the trigonal prismatic sites $P1$ and $P2$ [13], the La^{3+} ions occupy exclusively the sites $P2$, namely one third of them, forming a 2-dimensional superstructure of $\sqrt{3}a\times\sqrt{3}a$ type. The superstructure is analogous to that of $Sr_{0.35}CoO_2$, found by means of electron diffraction recently [20]. The deviation from the ideal stoichiometry $La_{1/3}CoO_2$ introduces extra carriers (formally 0.10 hole *per* Co) into the diamagnetic LS Co^{3+} matrix. The intrinsic $La_{0.30}CoO_2$ susceptibility associated with doped holes is dominated by a temperature independent term, $\chi_0=\chi_{core}+\chi_{VV}+\chi_{Pauli}\sim2.3\times10^{-4}\ \mathrm{emu\,mol^{-1}\,Oe^{-1}}$, when only about 0.01 hole *per* Co might be present as localized Co^{4+} state, giving rise to Curie type susceptibility $\chi=C/T$. As concerns the interpretation of the temperature independent term χ_0, the main uncertainty is connected with a Van Vleck orbital term χ_{VV}. Supposing localized model of Co^{3+} and Co^{4+} valence states, the orbital paramagnetism of Co^{3+} is determined by the distance $\Delta\sim2.7$ eV between the empty e_g and the occupied t_{2g} levels in the CoO_6 octahedra [18,21]. For Co^{4+} in trigonally distorted octahedron like in Na_xCoO_2, an anisotropic orbital contribution follows, determined by the distance $\Delta\sim0.4$ eV between the empty a_{1g} and occupied e_g' levels of the split t_{2g} manifold (see e.g. [22]). In a sum one gets $\chi_{VV}\sim2\times10^{-4}\ \mathrm{emu\,mol^{-1}\,Oe^{-1}}$ and we anticipate a similar value also for

band model though the calculation in that case is nontrivial [23]. Indeed, such estimate of the orbital paramagnetism for $La_{0.30}CoO_2$ is very close to Van Vleck component reported for the nominally Co^{3+} pure compound Na_1CoO_2—$\chi_{VV}=1.5\times10^{-4}$ emu mol^{-1} Oe^{-1} [24]. Adopting the same χ_{VV} value and calculated diamagnetic component $\chi_{core}=-0.4\times10^{-4}$ emu mol^{-1} Oe^{-1} for $La_{0.30}CoO_2$, we get for Pauli susceptibility a value $\chi_{Pauli}=\chi_0-\chi_{VV}-\chi_{core}\sim1.2\times10^{-4}$ emu mol^{-1} Oe^{-1}. This corroborates the electronic structure calculations. The calculated DOS at Fermi level, $N(E_F)=34$ Ry *per* f.u.$=6.5\times10^{22}$ eV^{-1} cm^{-3}, in fact gives a somewhat lower value $\chi_{Pauli}\sim0.8\times10^{-4}$ emu mol^{-1} Oe^{-1}, but this derivation does not take into account an enhancement of Pauli susceptibility due to electronic correlations. Using the same DOS, the calculated value of the electronic heat coefficient is $\gamma=0.006$ J K^{-2} mol^{-1}, in a reasonable agreement with the experimentally determined value $\gamma=0.0088$ J K^{-2} mol^{-1}.

Let us turn now to transport properties. The thermopower measurements are generally insensitive to the sample morphology, and the values observed on $La_{0.30}CoO_2$ are without doubt intrinsic. It is of interest that the temperature course of thermopower, which starts with a linear rise at low temperature and saturates above 600 K at a large value, does not differ much from what is generally observed in thermoelectric layered cobaltates of metallic character. According to recent theoretical calculations, the mentioned behavior of thermopower may originate in a peculiar shape of the a_{1g} band (the so-called "pudding mold") and can be explained within standard Boltzmann transport equations for metals [25,26].

In spite of all these signatures of Pauli metal, the DC conductivity in $La_{0.30}CoO_2$ shows localized features, characteristic for VRH. This behavior may have two origins. One is granular character of the sample where conduction can occur by quantum tunneling between metallic grains. For such transport, Efros–Shklovskii law $\ln\rho(T)\sim T^{-1/2}$ generally applies, irrespective the 3- or 2-dimensionality of intergrain paths [27,28]. Present data point, however, to another microscopic mechanism, namely Anderson localization at lattice disorder (the problem of mobility edge). In that case, Mott's law $\ln\rho(T)\sim T^{-1/3}$ is relevant for 2-dimensional transport. Such functional dependence is obeyed in $La_{0.30}CoO_2$ over a surprisingly broad temperature region, at least up to 400 K. We note that a similar $T^{-1/3}$ law was reported recently for the Y-substituted misfit cobaltate $Ca_3Co_4O_9$ upon reduction of hole doping by Y substitution for Ca [29].

The transition from the extended eigenfunctions in $Na_{0.90}CoO_2$ to localized ones in $La_{0.30}CoO_2$ can occur due to several reasons. Firstly, the obtained lanthanum composition 0.30(1) includes a certain error, which means that the actual carrier concentrations may be lower than the assumed 0.10 hole *per* Co. Secondly, the mobility of carriers may be critically influenced by important charge defects associated with some randomness of La^{3+} distribution. The static character of such defects and extreme rigidity of the CoO_2 conducting layers are possibly responsible for exceptionally large temperature domain of the VRH regime. The pronounced role of charge disorder in $La_{0.30}CoO_2$ is also manifested in much lower thermal conductivity compared to that in $Na_{0.75}CoO_2$ and $Na_{0.90}CoO_2$ samples—see Fig. 6c.

The position of the $La_{0.30}CoO_2$ at the itinerant-to-localized threshold may question simple theoretical considerations used in the analysis of its electric and magnetic properties. One of the unexpected results is the concurrence of Pauli susceptibility and Mott's VRH character of conduction. In our opinion, this need not represent any controversy if charge carriers are in the Anderson localized levels. These are multicenter states, which are spin-paired in the absence of applied magnetic field. Basic formulas in metal physics, which depend solely on the density of states, like that for Pauli susceptibility or electronic heat, are thus directly applicable. Anyway, there are a lot of issues for further investigation, particularly Hall measurements on $La_{0.30}CoO_2$ and the preparation and basic characterization of related rare-earth systems, which are under study.

Acknowledgments

This study was performed under the financial support by of the Grant Agency of the Czech Republic within the Project no. 203/09/1036. Part of the work was supported by Project No. 202/09/0421 of the Grant Agency of the Czech Republic.

References

[1] L. Viciu, J.W.G. Bos, H.W. Zandbergen, Q. Huang, M.L. Foo, S. Ishiwata, A.P. Ramirez, M. Lee, N.P. Ong, R.J. Cava, Phys. Rev. B 73 (2006) 174104.
[2] H.W. Zandbergen, M. Foo, Q. Xu, V. Kumar, R.J. Cava, Phys. Rev. B 70 (2004) 024101.
[3] M. Roger, D.J.P. Morris, D.A. Tennant, M.J. Gutmann, J.P. Goff, J.-U. Hoffmann, R. Feyerherm, E. Dudzik, D. Prabhakaran, A.T. Boothroyd, N. Shannon, B. Lake, P.P. Deen, Nature (London) 445 (2007) 631.
[4] M. Lee, L. Viciu, L. Li, Y. Wang, M.L. Foo, S. Watauchi, R.A. Pascal jr., R.J. Cava, N.P. Ong, Nat. Mat. 5 (2006) 537.
[5] L.M. Helme, A.T. Boothroyd, R. Coldea, D. Prabhakaran, A. Stunault, G.J. McIntyre, N. Kernavanois, Phys. Rev. B 73 (2006) 054405.
[6] B.L. Cushing, J.B. Wiley, J. Solid State Chem. 141 (1998) 385.
[7] Y.Q. Guo, J.L. Luo, G.T. Liu, H.X. Yang, J.Q. Li, N.L. Wang, D. Jin, T. Xiang, Phys. Rev. B 74 (2006) 155129.
[8] R. Ishikawa, Y. Ono, Y. Miyazaki, T. Kajitani, Jpn. J. Appl. Phys. 41 (2002) L337.
[9] Medium resolution neutron powder diffractometer MEREDIT, ⟨http://neutron.ujf.cas.cz/meredit⟩.
[10] J. Rodríguez-Carvajal, Physica B 192 (1993) 55 http://www.ill.eu/sites/fullprof.
[11] J. Hejtmánek, Z. Jirák, M. Maryško, C. Martin, A. Maignan, M. Hervieu, B. Raveau, Phys. Rev. B 60 (1999) 14057.
[12] P. Blaha, K. Schwarz, G.K.H. Madsen, D. Kvasnicka, J. Luitz, WIEN2k, An Augmented Plane Wave+Local Orbitals Program for Calculating Crystal Properties, Technische Universität, Wien, 2001.
[13] Q. Huang, M.L. Foo, R.A. Pascal Jr., J.W. Lynn, B.H. Toby, Tao He, H.W. Zandbergen, R.J. Cava, Phys. Rev. B 70 (2004) 184110.
[14] P. Mendels, D. Bono, J. Bobroff, G. Collin, D. Colson, N. Blanchard, H. Alloul, I. Mukhamedshin, F. Bert, A. Amato, A.D. Hillier, Phys. Rev Lett. 94 (2005) 136403.
[15] D.J. Singh, Phys. Rev. B 61 (2000) 13397.
[16] T. Mousavand, T. Naka, K. Sato, S. Ohara, M. Umetsu, S. Takami, T. Nakane, A. Matsushita, T. Adschiri, Phys. Rev. B 79 (2009) 144411.
[17] Y. Ichiyanagi, Y. Kimishima, S. Yamada, J. Magn. Magn. Mater. (2004) 272–276, e1245 (2004).
[18] W.L. Roth, J. Phys. Chem. Solids 25 (1964) 1.
[19] T.F. Schulze, M. Brühwiler, P.S. Häfliger, S.M. Kazakov, Ch. Niedermayer, K. Mattenberger, J. Karpinski, B. Batlogg, Phys. Rev. B 78 (2008) 205101.
[20] H.X. Yang, Y.G. Shi, Y.Q. Guo, X. Liu, R.J. Xiao, J.L. Luo, J.Q. Li, Mater. Res. Bull. 42 (2007) 94.
[21] J.S. Griffith, L.E. Orgel, Trans. Farad. Soc. 53 (1957) 601.
[22] H. Alloul, I.R. Mukhamedshin, N. Blanchard, G. Collin, J. Phys. IV France 131 (2005) 27.
[23] R. Kubo, Y. Obata, J. Phys. Soc. Jpn. 11 (1956) 547.
[24] G. Lang, J. Bobroff, H. Alloul, P. Mendels, N. Blanchard, G. Collin, Phys. Rev. B 72 (2005) 094404.
[25] K. Kuroki, R. Arita, J. Phys. Soc. Jpn. 76 (2007) 083707.
[26] D.J. Singh, D. Kasinathan, J. Electron. Mater. 36 (2007) 736.
[27] P. Sheng, Philos. Mag. B 65 (1992) 357.
[28] C.-H. Lin, G.Y. Wu, Thin Solid Films 397 (2001) 280.
[29] Y. Wang, Y. Sui, J. Cheng, X. Wang, W. Su, X. Liu, H.-J. Fan, J. Phys. Chem. C 114 (2010) 5174.